

# Towards Mott design by $\delta$ -doping of strongly correlated titanates

Frank Lechermann and Michael Obermeyer

I. Institut für Theoretische Physik, Universität Hamburg, D-20355 Hamburg, Germany

**Abstract.** Doping the distorted-perovskite Mott insulators  $\text{LaTiO}_3$  and  $\text{GdTiO}_3$  with a single SrO layer along the [001] direction gives rise to a rich correlated electronic structure. A realistic superlattice study by means of the charge self-consistent combination of density functional theory with dynamical mean-field theory reveals layer- and temperature-dependent multi-orbital metal-insulator transitions. An orbital-selective metallic layer at the interface dissolves via an orbital-polarized doped-Mott state into an orbital-ordered insulating regime beyond the two conducting  $\text{TiO}_2$  layers. We find large differences in the scattering behavior within the latter. Breaking the spin symmetry in  $\delta$ -doped  $\text{GdTiO}_3$  results in blocks of ferromagnetic itinerant and ferromagnetic Mott-insulating layers which are coupled antiferromagnetically.

## 1. Introduction

In view of future technological applications, the investigation of oxide heterostructures provides the possibility for exploring novel composite materials beyond nature's original conception (see e.g. [1, 2, 3]) for reviews). Additionally, this research extends the concept of materials design towards the realm of strongly correlated systems. Many of the essential heterostructure building blocks either harbor partially-filled transition-metal  $d$ -shells already in their bulk configuration (e.g.  $\text{LaTiO}_3$ ,  $\text{LaVO}_3$ ,  $\text{GdTiO}_3$ , etc.) or display such partial filling due to interface doping (e.g. for  $\text{SrTiO}_3$ ). Therefore weakly-screened Coulomb interactions may give rise to explicit many-body effects that eventually govern the materials physics. Unusual metallicity from combining bulk band insulators, emergent magnetic order, superconductivity or large thermopower are only a few fascinating phenomena that occur in the interfacing regions. Engineering such structured matter allows for a direct manipulation of systems in or close to the Mott-critical regime, i.e. offers the potential for *Mott design*. As a specific realization thereof, the  $\delta$ -doped oxide heterostructures [4, 5, 6, 7], i.e. introducing well-defined impurity monolayers into a given host oxide compound, recently emerged as a canonical method to create challenging electronic states from experimental fabrication. Especially the  $\delta$ -doping of Mott insulators [8, 9, 10, 11] not only has relevance in the designing context, but furthermore sheds light on the generic physics of the realistic doped-Mott state in a controlled way without the usual complications arising from disorder and other features of random impurity doping.

In this work we use a first-principles many-body approach to investigate the  $\delta$ -doping of the Mott insulators  $\text{LaTiO}_3$  (LTO) and  $\text{GdTiO}_3$  (GTO). The bulk materials are examples of two qualitatively different trends within the series of perovskite-like  $R\text{TiO}_3$  compounds ( $R$ =rare-earth element) [12] with  $\text{GdFeO}_3$ -type distortion. While for smaller rare-earth ionic radius (Yb, Y, Gd) the systems become ferromagnetic at low temperature, for larger radius (Sm, Nd, La) the materials are  $G$ -type antiferromagnetic in the crystallographic  $a$  direction upon cooling. For GTO the Curie temperature is 36K and the Néel temperature of LTO amounts to 146K. An increasing deviation of the Ti-O-Ti bond angle from  $180^\circ$  from La to Y is key to the change of magnetic ground state among the titanates [13, 14, 15, 16, 17]. The crucial low-energy electron states are dominated by the threefold of  $\text{Ti}(t_{2g})$  orbitals, with a nominal filling of one electron. Numerous theoretical studies are devoted to reveal the electronic structure of these bulk Mott insulators [18, 19, 20, 21, 22, 23, 24]. Especially the very detailed ab-initio study of Pavarini *et. al* [23] covers many aspects of the representants  $\text{LaTiO}_3$  and  $\text{YTiO}_3$ , from the generic band structure to crystal-field/tight-binding considerations, up to the inclusion of correlation effects. The latter are shown to be important in driving significant orbital ordering in these  $3d^1$  materials, which renders other orbital-degenerate modelings questionable.

Main intention here is to shed light on the correlation physics of  $\delta$ -doped heterostructures as well as to promote the  $R\text{TiO}_3$  physics to the next level by investigating the behavior from doping with a single SrO layer. We thereby concentrate on the temperature regimes above the bulk magnetic ordering. Two main question arise in the latter scenario: the first one concerns the appearance of metallization via the non-random hole doping, and if it sets in, the characterization in terms of the multi-orbital Ti manifold and its layer dependence. When a (layer-dependent) Mott state is reached, its possible deviation from the known bulk Mott-insulating state is secondly of key interest. The clarification of the correlated electronic structure in this

canonical structure case is highly relevant for the understanding of other layerings and possible applications, e.g. in the area of solar cells [25].

Using the charge self-consistent combination of density functional theory (DFT) with dynamical mean-field theory (DMFT) in a superlattice architecture we indeed reveal a very rich electronic-structure phenomenology. Layer-dependent multi-orbital metal-insulator transitions via  $\delta$ -doping are identified for the case of SrO/LTO and SrO/GTO heterostructures, that involve three different electronic regimes. With increasing distance to the doping layer, an  $xy$ -dominated metallic state settling right at the interface is replaced by an orbital-polarized doped-Mott metallic layer which transforms to bulk-modified insulating Mott layers. Embedding such complex electron states within oxide heterostructures opens the door for many ways of manipulations and can lead to the identification of building blocks for new devices.

## 2. Theoretical framework

On the level of the local density approximation (LDA) to density functional theory (DFT), a mixed-basis pseudopotential framework [26, 27] is applied for the structural optimization of the  $\delta$ -doped supercells and the basic electronic structure investigation. Norm-conserving pseudopotentials as well as a combined basis of plane waves and localized functions for Ti( $3d$ ) and O( $2s2p$ ) is utilized. The latter allow for a moderate plane-wave cutoff energy  $E_{\text{cut}}=13\text{Ryd}$  for the demanding supercell calculations, which are based on a  $5\times 5\times 3$   $k$ -point mesh in reciprocal space. Though  $f$ -electrons can be also treated also in many-body bulk computations, we here aim for novel correlations effects dominantly from first-principles  $3d$  electrons in challenging heterostructure architectures. Thus effects of possible  $4f$  states are captured approximately. In La those states are unoccupied in the atom and form empty conduction states in LTO. One may neglect them for the present purpose to a good approximation in the pseudopotential construction and the localized-function basis. Contrary to the neighboring band-insulating  $\text{EuTiO}_3$  compound with  $\text{Eu}^{2+}$  and  $\text{Ti}^{4+}$ , GTO harbors  $\text{Gd}^{3+}$  and  $\text{Ti}^{3+}$ . This shifts the half-filled  $4f$  shell (occupation 7 electrons) shell of Gd further down in energy and with an assumed large intra-orbital Coulomb interaction this local manifold, deep in energy, has no quasiparticle contribution at low energy. Hence the  $\text{Gd}(4f)$  shell is not of eminent importance in  $\text{GdTiO}_3$  and is here put in the pseudopotential frozen core.

Full local electronic correlation effects beyond the static (i.e. LDA, LDA+U) realm are taken care of by the dynamical mean-field theory (DMFT) within the framework of charge self-consistent DFT+DMFT [28, 29, 30]. The multi-site and -orbital correlated subspace where explicit Coulomb interactions are treated on the many-body level is here defined by the  $t_{2g}$ -like low-energy crystal-field (cf) bases of the various Ti ions in the given structures. It is obtained by tailored projected local orbitals [31, 32, 33] based on a set of low-energy Kohn-Sham (KS) states. The orbital projections are given by linear combinations of the original ( $xz$ ,  $yz$ ,  $xy$ ) functions that diagonalize the local  $t_{2g}$ -like  $3\times 3$  orbital density matrix on each Ti ion, respectively. In case of the bulk compounds, the 12 low-energy KS bands close to the Fermi level are used to facilitate the projection. All Ti ions are equivalent by symmetry in the bulk  $\text{GdFeO}_3$  structure and the site-dependent projections can be chosen such that a single  $3\times 3$  self-energy matrix  $\Sigma(\omega)$  is converged. For the  $\delta$ -doped compounds, a multi-site DFT+DMFT scheme is put into practise with 5 inequivalent Ti ions in the chosen supercells (see sections 3 and 5). There a KS manifold of 60 low-energy bands

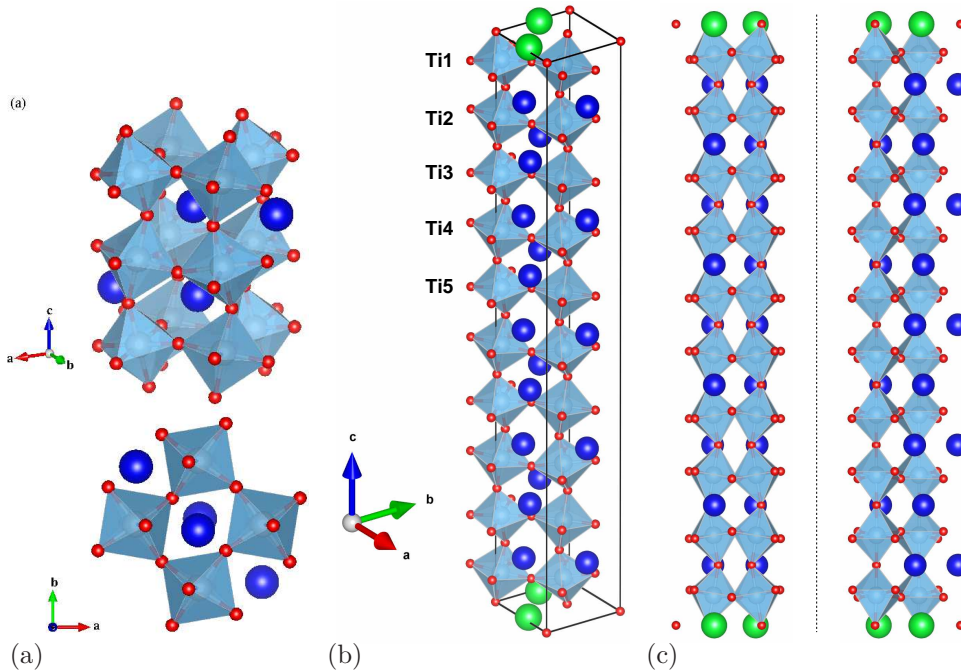


**Figure 1.** Crystal structures exemplified for the LTO case. (a) bulk LTO in perspective view (top) and along the  $c$ -axis (bottom). (b,c)  $\delta$ -doped SrO/LTO: (b) in perspective view, (c) along  $a$ -axis (left) and along  $b$ -axis (right). La (blue), Sr (green), Ti (gray), O (red).

enters the projection.

A rotational-invariant three-orbital Hubbard Hamiltonian in Slater-Kanamori parameterization is applied on each Ti site. The intra-orbital Coulomb interaction is chosen as  $U=5\text{eV}$  and the Hund's exchange as  $J_{\text{H}}=0.64\text{eV}$ , identical to former LDA+DMFT studies of bulk titanates [21, 23]. Continuous-time quantum Monte Carlo in the hybridization expansion [34, 35, 36, 37] is utilized to solve the DMFT impurity problems. At each correlated Ti site  $i$  and orbital  $m$  a double-counting (DC) correction of the fully-localized form [38] making use of the local particle-number operator  $n_i$ , i.e.  $\Sigma_{im\sigma}^{\text{DC}}=U(\langle n_i \rangle - 1/2) - J_{\text{H}}(\langle n_{i\sigma} \rangle - 1/2)$  with  $\sigma=\uparrow, \downarrow$ , is applied to the self-energy in the complete charge self-consistent convergency cycle. The resulting local and total spectral functions are derived from analytical continuation of the Green's functions in Matsubara space via the maximum-entropy method.

Note that different or larger correlated subspaces, e.g. by including O( $2p$ )-dominated KS band states in the projection, are possible and currently under investigation for oxide bulk Mott insulators [39, 40]. But since our focus is on the challenging large-scale heterostructure problem where such recent extensions are very expensive, we work in minimal  $t_{2g}$ -based correlation framework. In an initial study [10], the  $\delta$ -doping of LTO with a single SrO layer was in part already investigated within DFT+DMFT. But there the inplane lattice constant  $a=b$  of bulk SrTiO<sub>3</sub>, a site-averaged DC as well as cubic  $t_{2g}$  projections, i.e. not adapted to the local crystal-field eigenbasis, were used. Albeit valuable insight was obtained, the correlation physics of such heterostructures is rather sensitive to details and therefore we here advance in

the modelling. Concerning the notorious double-counting term, a site-dependent DC correction is more tailored to the real-space problem of correlated sites with different distances to existing interfaces.

### 3. Crystal-structure considerations

Bulk crystal structures of LTO and GTO with  $Pbnm$  space group are experimentally well studied and we here utilize available x-ray diffraction data [12] (see Fig. 1a). Relevant parameters of the distorted perovskite structure with 4 formula units in the primitive cell are tilt and in-plane rotation of the  $\text{TiO}_6$  octahedra, both with respect to the  $c$ -axis. The deviations from the perovskite structure are larger in GTO. A measure thereof is given by the angles between  $\text{Ti-O1-Ti}$  and  $\text{Ti-O2-Ti}$ , where O1 marks the apical oxygen ion and O2 the one in the basal plane of the octahedron. The latter plane is furthermore distorted differently in both structures. While in LTO that distortion is rectangular, in GTO it is of parallelogram shaping [12].

To facilitate the  $\delta$ -doping scenario, a single SrO layer is inserted in the hosting titanates within a periodic superlattice architecture in  $[001]$  direction, respectively. Along the  $c$ -axis the supercells (see Fig. 1b) consist of 10  $\text{TiO}_2$  and 9  $\text{La(Gd)O}$  host layers inbetween the SrO monolayers. This amounts to a separating distance of about 4nm between the latter. A  $\sqrt{2}\times\sqrt{2}$  unit is chosen in lateral in-plane direction to allow for the  $\text{TiO}_6$  octahedral tilts/rotations and distortions, i.e. each  $\text{TiO}_2$  layer includes two Ti sites. Thus there are 20 Ti ions in these supercells with a total number of 100 atoms. For the lattice parameters  $a$ ,  $b$  and  $c$  the experimental bulk LTO/GTO

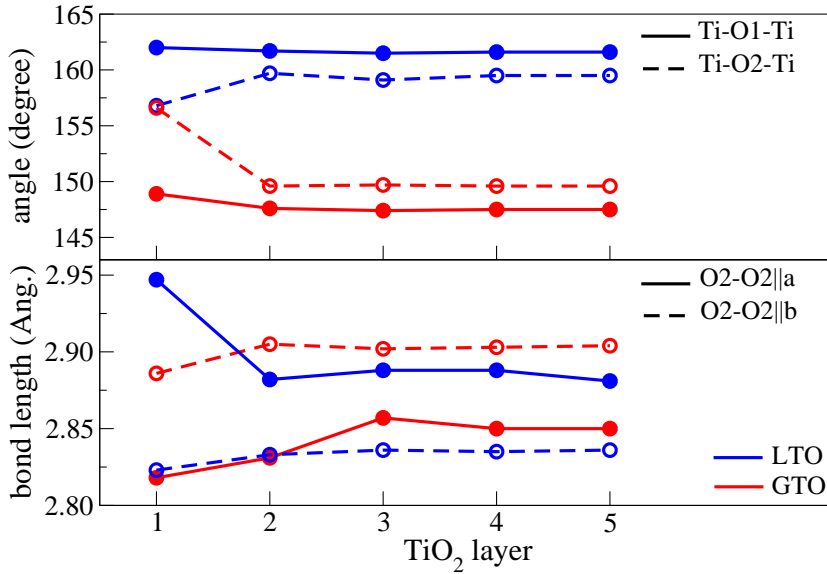


**Figure 2.** Relevant layer-dependent cell-internal parameters for the  $\delta$ -doped structures within LDA. Top: bond angles  $\text{Ti-O-Ti}$ . Bottom: bond lengths  $l$  in the basal plane of the  $\text{TiO}_6$  octahedra. The experimental reference values for the stoichiometric bulk compounds are  $\angle\text{Ti-O1-Ti}=153.9^\circ$  ( $143.9^\circ$ ) and  $\angle\text{Ti-O2-Ti}=153.3^\circ$  ( $145.8^\circ$ ) for LTO(GTO) as well as  $l(\text{O2-O2}||a)=2.94(2.90)\text{\AA}$  and  $l(\text{O2-O2}||b)=2.85(2.91)\text{\AA}$  for LTO(GTO) [12].

values are used and the atomic positions are obtained from minimizing the atomic forces within LDA down to 10 mRyd/a.u. per site. Note that the method of choice for structural optimization in low-symmetry correlated materials, i.e. LDA, GGA or static DFT+U [41] is still open and a matter of debate.

It is well known that the tilts, rotations and distortions of the  $\text{TiO}_6$  octahedra in the  $R\text{TiO}_3$  series are crucial for the Mott insulating as well as the magnetic state. Thus the changes thereto by the SrO doping layer may have strong influence on the resulting electronic structure. The relaxed structural data is summarized by providing layer-dependent bond angles and bond lengths (see Fig. 2). In general, the LDA bond angles in the  $\delta$ -doped structures turn out somewhat larger than the experimental values for the bulk stoichiometric systems. But the hierarchy, marking GTO with stronger tilts and rotations of the  $\text{TiO}_6$  octahedra, remains intact. For both structures, the differences in tilts and rotations are strongest close to the SrO doping layer. The octahedral tilt and rotation are related to the Ti-O1-Ti, Ti-O2-Ti angles. The former(latter) angle is somewhat enhanced(reduced) close the interface in the LTO case. In the GTO case both angles are shifting in the direction of the non-distorted value of  $180^\circ$  when approaching the interface. Note that these overall smaller tilts compared to the bulk cases are in qualitative agreement with recent measurements using scanning transmission electron microscopy on SrO quantum wells in GTO [42]. The LDA bond lengths between the O2 ions in the octahedral basal plane are in general somewhat lower than in the experimental bulk structures. Close to the interface the rectangular distortion is enhanced in the LTO case, while for  $\delta$ -doped GTO some shrinking of the basal plane may be noticed.

Our structural data is in line with recent GGA+U calculations by Chen *et al.* where a smaller supercell for  $\delta$ -doped GTO along the [001] direction was used. On the experimental side, Zhang *et al.* [42, 8, 43] studied the structural modifications due to doping GTO with a SrO monolayer, but using a different interface geometry. There it is defined by the directions [110] and [001], i.e. the  $c$ -axis parallel to the interface and  $a, b$  inclined. Whereas in the present work the interface is given by the directions [100] and [010]. The observation of somewhat smaller octahedral tilts right at the interface agrees between theory and experiment. Still the geometry influence on the electronic structure may be significant, e.g. because of orbital-ordered Mott(-like) states with a unique directional character.

#### 4. Electron states in bulk $\text{LaTiO}_3$ and bulk $\text{GdTiO}_3$

This section summarizes the electronic structure of the bulk compounds to set the stage for comparison with the  $\delta$ -doped cases. The La- and Gd-titanate are well-defined metals in the conventional Kohn-Sham representation of DFT. Both display an  $t_{2g}$ -like low-energy manifold close to the Fermi level  $\varepsilon_F$  in LDA (see Fig. 3) of bandwidths  $W_{\text{LTO}}=1.9\text{eV}$  and  $W_{\text{GTO}}=1.8\text{eV}$ . The GTO density of states (DOS) at  $\varepsilon_F$  is larger than the LTO one and the  $t_{2g}$ - $e_g$  gap in the unoccupied energy region is also increased for the former. Therefrom the Gd compound is somewhat stronger susceptible to correlation effects than the La one.

The LTO local crystal-field basis from the projected local orbitals reads (note that phases differ on the various Ti sites)

$$\begin{pmatrix} |1\rangle \\ |2\rangle \\ |3\rangle \end{pmatrix} = \begin{pmatrix} 0.710 & 0.274 & -0.648 \\ 0.262 & 0.752 & 0.605 \\ 0.653 & -0.600 & 0.462 \end{pmatrix} \begin{pmatrix} xz \\ yz \\ xy \end{pmatrix}, \quad (1)$$

with level energies  $\varepsilon_{\text{cf}}^{(1)}=483\text{meV}$ ,  $\varepsilon_{\text{cf}}^{(2)}=379\text{meV}$  and  $\varepsilon_{\text{cf}}^{(3)}=491\text{meV}$ . Lowest in energy is state  $|2\rangle$  with dominant  $yz$  and weakest  $xz$  contribution, in qualitative agreement with the previous study [23] based on linear/ $N$ th-order muffin-tin orbital methods in the atomic-sphere approximation. Crystal-field splittings  $\Delta_{2,3}=\varepsilon_{\text{cf}}^{(2,3)} - \varepsilon_{\text{cf}}^{(1)}$  of the order of  $100\text{meV}$  turn out to be somewhat smaller in the present work. The local DOS of these states is plotted in Fig. 3 and shows no very significant orbital discrimination in its shape. No sizeable orbital polarization is seen on the LDA level, the single  $\text{Ti}(3d)$  electron is shared among the adapted states.

For GTO the corresponding local crystal-field basis is given by

$$\begin{pmatrix} |1\rangle \\ |2\rangle \\ |3\rangle \end{pmatrix} = \begin{pmatrix} 0.639 & 0.449 & 0.625 \\ 0.707 & -0.664 & -0.245 \\ -0.305 & -0.598 & 0.741 \end{pmatrix} \begin{pmatrix} xz \\ yz \\ xy \end{pmatrix}, \quad (2)$$

with level energies  $\varepsilon_{\text{cf}}^{(1)}=319\text{meV}$ ,  $\varepsilon_{\text{cf}}^{(2)}=483\text{meV}$  and  $\varepsilon_{\text{cf}}^{(3)}=456\text{meV}$ . State  $|1\rangle$  with lowest energy is here a more balanced combination of the original  $t_{2g}$  orbitals, with weakest contribution from  $yz$ . The crystal-field splittings are similar to the LTO case, with a small increase in numbers. Stronger orbital discrimination is visible on the LDA level, i.e. the local DOS of the  $|1\rangle$  state marks not only a smaller bandwidth but has a significant larger value at the Fermi level. This leads to some orbital polarization towards  $|1\rangle$  in the single-electron share.

Figure 4 shows the obtained effective  $t_{2g}$  orbitals for both titanates. As within other downfolding schemes applied to transition-metal oxides [23, 44], the Wannier-like functions exhibit significant weight on the nearby oxygen ions, as expected via the

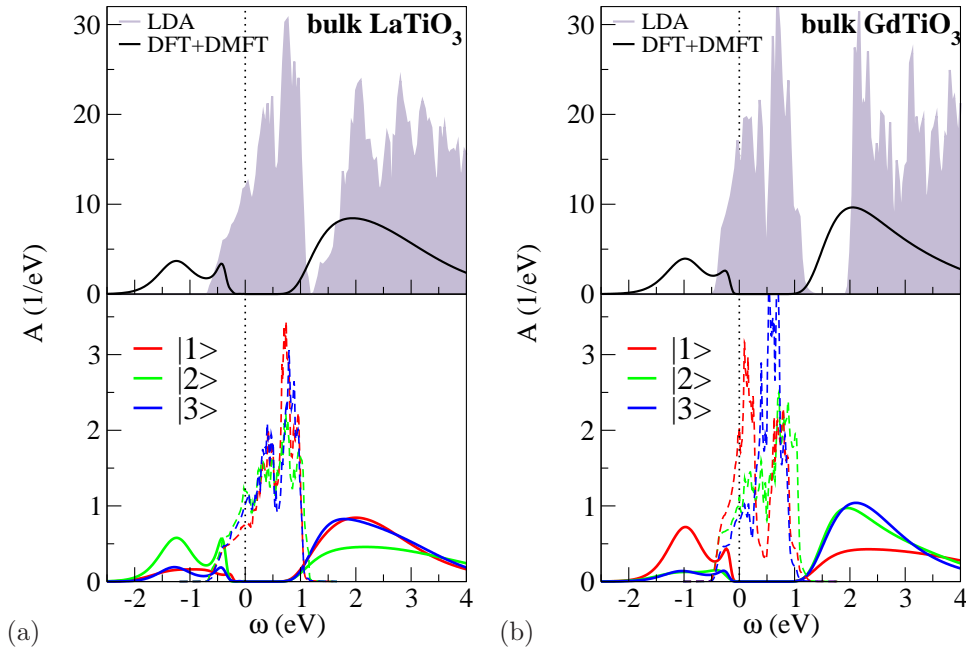


**Figure 3.** Spectral-function comparison between LDA and DFT+DMFT ( $T=290\text{K}$ ) for the bulk case of (a) LTO and (b) GTO. Top: total spectrum, bottom: local orbital-resolved spectrum with dashed lines for the LDA result.

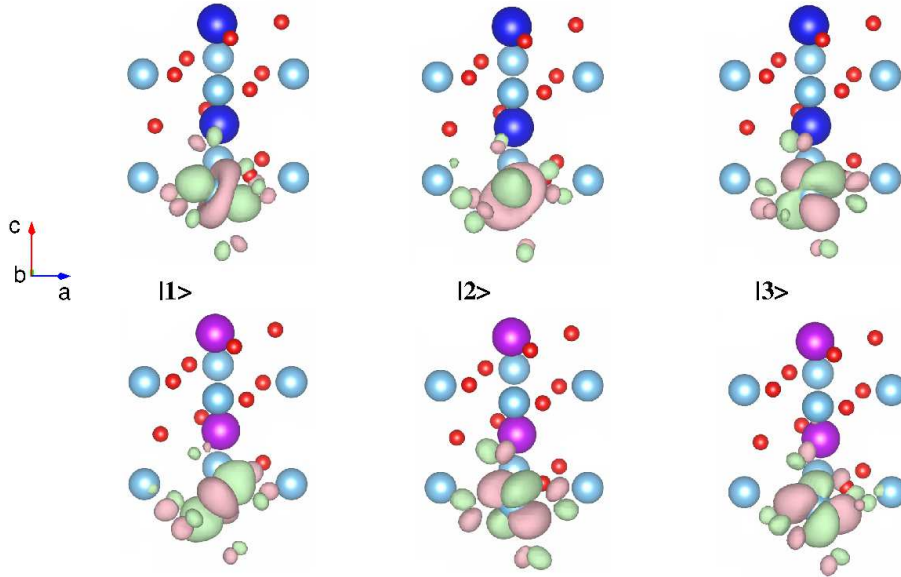


**Figure 4.** Crystal-field orbitals from the projection formalism for the bulk cases of LTO (top) and GTO (bottom). La (blue), Gd (violet), Ti (gray), O (red).

projection from low-energy KS states. Note that though the projection orbitals are atomic-like functions [32], the resulting correlated subspace is composed of Wannier-like functions due to the projection onto selected KS states. Concerning the lowest-energy crystal-field orbitals, the  $|2\rangle$  state of LTO is mainly oriented along the  $b$ -axis, while the  $|1\rangle$  state of GTO is aligned along the  $a$ -axis. Furthermore the GTO  $|3\rangle$  orbital has a clearer in-plane  $xy$  character, whereas a clear resemblance thereof is lacking in LTO.

The electronic structure of these compounds is modified substantially within DFT+DMFT. For both materials the experimental room-temperature Mott-insulating state is confirmed (see Fig. 3). Lower Hubbard bands are located at  $\sim 1.2\text{eV}$  for LTO and at  $\sim 1\text{eV}$  for GTO. In our present scheme the charge gaps amount to  $\Delta_{\text{LTO}}^g \sim 0.5\text{eV}$  and  $\Delta_{\text{GTO}}^g \sim 0.8\text{eV}$ . While the latter value is in good agreement with experimental data of about  $0.75\text{eV}$  [45], our result for the LTO value is larger than  $\Delta_{\text{LTO}}^g \sim 0.2\text{--}0.3\text{eV}$  from experiment [46, 47]. A smaller theoretical charge gap was obtained in previous non-charge-self-consistent studies [21] with similar correlated subspace and same interaction parameters, but at much higher temperature  $T=1200\text{K}$ . Recent DFT+DMFT with larger correlated subspace and including the unoccupied  $4f$  state reaches a smaller value also close to room temperature [39]. Substantial orbital polarization takes place in the Mott state, with dominant filling of the effective  $|2\rangle$  ( $|1\rangle$ ) orbital in LTO (GTO). The occupation numbers for ( $|1\rangle$ ,  $|2\rangle$ ,  $|3\rangle$ ) read (0.22, 0.59, 0.19) for LTO and (0.66, 0.18, 0.16) for GTO. Hence with correlations, close to  $2/3$  of the single  $t_{2g}$  electron resides in lowest crystal-field level.



## 5. Electron states in $\delta$ -doped compounds without broken spin/charge symmetry

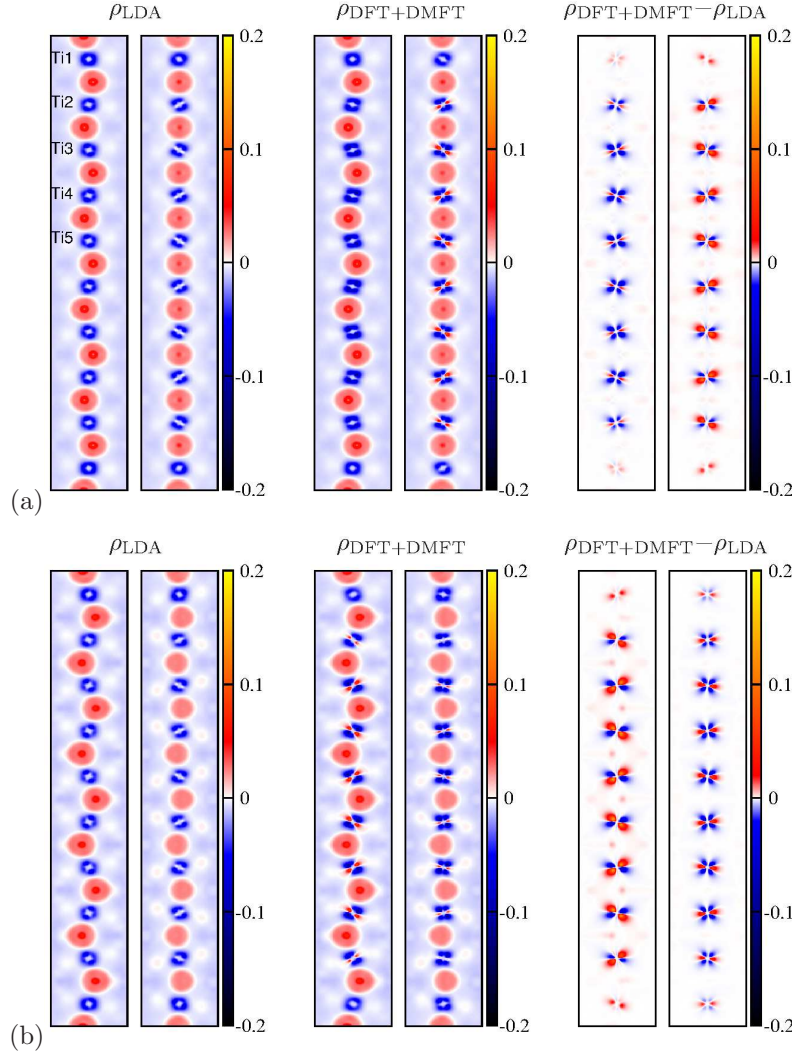
Realistic correlation effects from  $\delta$ -doping LTO and GTO are approached in a multi-site DFT+DMFT scheme. The 5 inequivalent Ti ions in the supercell structures allow for corresponding layer-dependent effective- $t_{2g}$  DMFT self-energies  $\Sigma 1-5$  beyond static considerations. In this section we first concentrate on the electronic structure without possible breaking of spin and charge symmetries, i.e. paramagnetic states as well as charge-balanced solutions. To this, no intra-layer discrimination of the both Ti ions per layer is performed, respectively. Symmetry-broken solutions for  $\delta$ -doped GTO will be discussed in section 6.

Table 1 provides the list of matrices, based on LDA calculations, transforming the original  $(xz, yz, xy)$  orbitals into the, now layer-dependent, crystal-field bases  $(|1\rangle, |2\rangle, |3\rangle)$ . The variations in the coefficients are largest between the groups (Ti1, Ti2) and (Ti3, Ti4, Ti5), but the classification of the effective orbitals remains stable across the different  $\text{TiO}_2$  layers. From the onsite level energies  $\varepsilon_{cf}$  of the effective crystal-field states it is seen that again the  $|2\rangle(|1\rangle)$  state is lowest on the Ti3-5 sites in the doped LTO(GTO) case, as found for the bulk Ti site. The level spacing on those three sites is also nearly identical to the bulk for GTO, whereas for the LTO case the energy difference is up to 60% larger. On Ti2 the level energies come already substantially closer compared to Ti3-5. Qualitative energetic changes occur for the  $\text{TiO}_2$  layer closest to the SrO doping layer: the Ti1 sites has state  $|3\rangle$ , with dominant  $xy$  contribution, lowest for both titanates types.

The single SrO layer induces hole doping in the  $3d^1$  titanates, trying to shift the

		$\delta$ -LTO				$\delta$ -GTO			
		$xz$	$yz$	$xy$	$\varepsilon_{cf}$	$xz$	$yz$	$xy$	$\varepsilon_{cf}$
Ti1	$ 1\rangle$	-0.930	0.212	-0.300	656	-0.735	0.227	-0.638	668
	$ 2\rangle$	-0.354	-0.739	0.573	663	-0.328	-0.944	0.041	730
	$ 3\rangle$	0.100	-0.639	-0.763	597	0.593	-0.240	-0.769	577
Ti2	$ 1\rangle$	0.943	0.322	0.086	569	0.746	-0.268	0.609	409
	$ 2\rangle$	-0.176	0.699	-0.693	428	0.362	0.932	-0.032	534
	$ 3\rangle$	-0.284	0.638	0.716	587	-0.559	0.245	0.792	508
Ti3	$ 1\rangle$	-0.984	0.168	0.056	545	0.718	0.321	0.617	387
	$ 2\rangle$	-0.165	-0.754	-0.636	387	0.324	-0.939	0.111	524
	$ 3\rangle$	-0.065	-0.635	0.770	577	0.616	0.120	-0.779	502
Ti4	$ 1\rangle$	-0.982	0.190	0.002	544	-0.715	-0.331	0.616	382
	$ 2\rangle$	-0.146	-0.759	0.634	390	-0.289	0.942	0.170	519
	$ 3\rangle$	0.122	0.622	0.773	578	-0.637	-0.057	-0.769	498
Ti5	$ 1\rangle$	-0.978	0.210	0.012	547	0.721	0.325	0.612	384
	$ 2\rangle$	-0.171	-0.758	-0.629	395	0.305	-0.942	0.140	521
	$ 3\rangle$	-0.123	-0.617	0.777	575	0.622	0.086	-0.779	499

**Table 1.** Layer-dependent Ti crystal-field bases within the projected local orbitals defining the correlated subspace for the  $\delta$ -doped compounds. The given  $3 \times 3$  matrices transform the  $(xz, yz, xy)$  orbitals to the tailored  $(|1\rangle, |2\rangle, |3\rangle)$  orbitals in the same manner as given in eqs. (1,2) for the respective bulk case. The quantities  $\varepsilon_{cf}$  denote the respective onsite level energies (in meV) for the resulting tailored orbitals.



**Figure 5.** Bond charge densities  $\rho = \rho_{\text{total}} - \rho_{\text{atomic}}$  for  $\delta$ -doped (a) LTO and (b) GTO. For each protocol, densities within (left) the  $ac$ -plane and (right) the  $bc$ -plane are given. The DFT+DMFT data is retrieved from calculations at  $T=290\text{K}$ .

nominal  $\text{Ti}^{3+}$  state towards  $\text{Ti}^{4+}$  as found in bulk  $\text{SrTiO}_3$ . Since the complete unit cell hosts ten  $\text{TiO}_2$  layers the doping amounts to 0.1 electrons per Ti ion. Figure 5 displays the resulting bond charge density (BCD) within LDA and DFT+DMFT. These densities are evaluated as differences between the obtained total charge density and the original overlaid atomic charge densities, thus reveal the key effects due to crystallization. One main BCD feature for the considered transition-metal-oxide compounds is the ionic charge transfer from titanium to oxygen. Beyond that the LDA BCD does not show much more deeper characteristics. The BCD from DFT+DMFT on the other hand clearly reveals the orbital polarization in the different crystallographic directions for LTO and GTO far from the SrO layer. A difference plot

visualizes this polarization readily as local correlation effects, i.e. onsite  $3d$  charge transfers. Especially in the GTO case, further correlation-induced charge transfer to oxygen ions occurs. Close to the SrO layer the orbital polarization is weak, mainly a minor additional charge transfer into that region from the interior within DFT+DMFT compared to LDA becomes visible.

Further details on the  $\delta$ -doped LTO correlated electronic structure are revealed from the  $k$ -summed one-particle spectral function  $A(\omega)=\sum_{\mathbf{k}} A(\mathbf{k},\omega)$ . The studied  $T$  range starts above 1000K and ends at 145K, close to the bulk Néel temperature. The total spectrum has metallic character for all investigated temperatures, but exhibits strong transfer of spectral weight to Hubbard peaks (see Fig. 6a). Compared to the bulk case, the centre of the lower Hubbard peak is shifted upwards to  $\sim 0.9$ -1eV. The quasiparticle (QP) peaks have significant  $T$  dependence, displaying bad-metal behavior at elevated temperatures. Only well below room temperature a clear

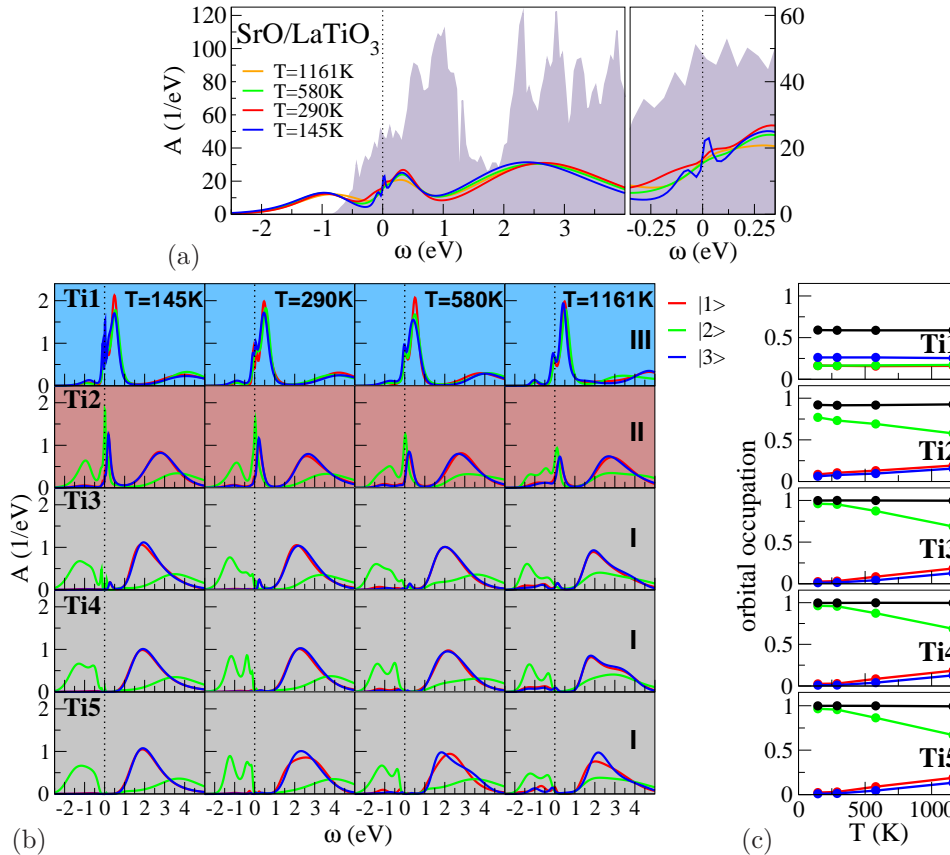


**Figure 6.**  $k$ -integrated spectral function  $A(\omega)$  for  $\delta$ -doped LTO from DFT+DMFT. (a) Total function compared to LDA (bluegrey), where  $A(\omega)$  builds on the 60 electron states from the bottom of the low-energy  $t_{2g}$  manifold. Left: blow-up around  $\varepsilon_F$ . (b) Local Ti-resolved functions, with three electronic regions: orbital-ordered Mott insulating (grey bg), orbital-polarized doped (lightred bg) and orbital-selective doped (lightblue bg). (c) Ti-resolved orbital fillings, black datapoints/line marks the respective total  $n$ .

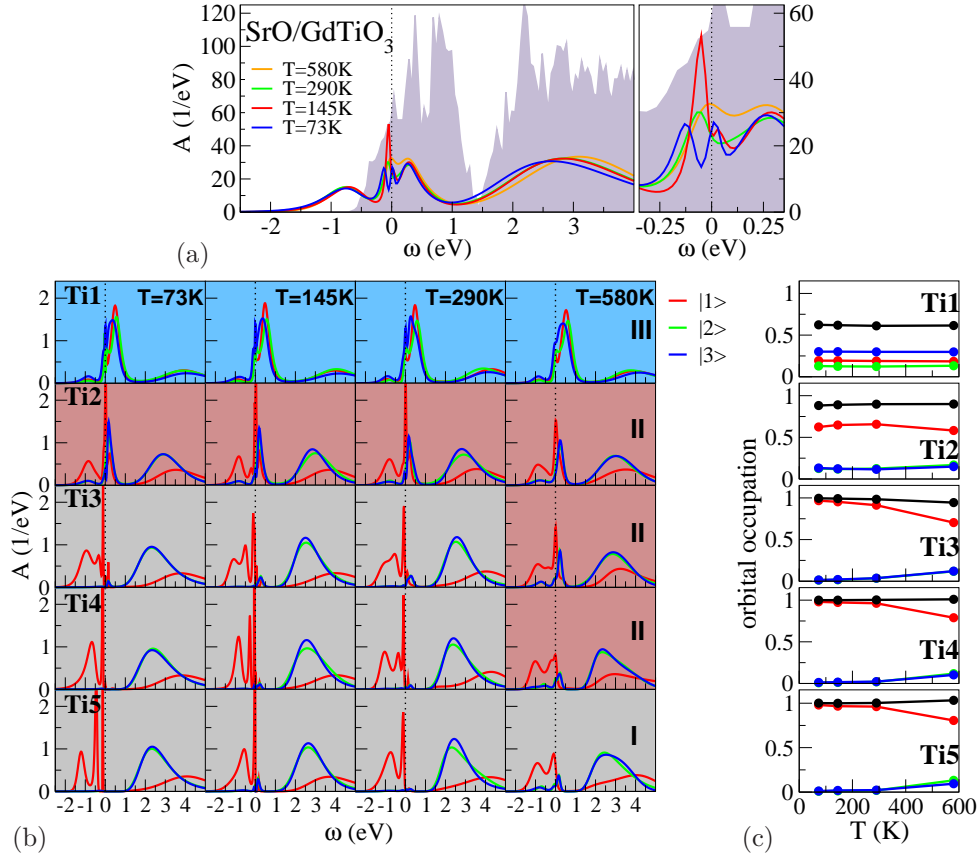


**Figure 7.**  $k$ -integrated spectral function  $A(\omega)$  for  $\delta$ -doped GTO from DFT+DMFT. The subfigures (a-c) are described as in Fig. 6.

resonance occurs at the Fermi level. A layer-dependent multi-orbital Mott transition is inferred from the local Ti-resolved  $A(\omega)$ . Its structure renders it possible to separate the  $\delta$ -doped electronic structure into three distinct regimes (see Fig. 6b): Far from the doping layer the material is in a *orbital-ordered Mott state* (I), with insulating layers derived from Ti3-5. Notably these Mott layers are still different from the bulk-LTO state. The orbital polarization towards (layer-dependent)  $|2\rangle$  is nearly complete already close to room temperature (compare also Fig. 6c), while in bulk LTO only about 2/3 of the single electron resides in state  $|2\rangle$ . This is in line with the finding of stronger energy separation of the onsite crystal-field levels in  $\delta$ -LTO (cf. Tab. 1). In addition, the local charge gap is somewhat reduced compared to the bulk value. For higher  $T$  the gaps are partially filled by incoherent excitations. The second regime (II) is built from the next-nearest  $\text{TiO}_2$  layer from the interface, an *orbital-polarized doped-Mott* layer with QPs at low energy. While the occupied part, including Hubbard and QP excitation, is dominated by  $|2\rangle$ , minor QP weight is shifted towards  $|1\rangle$ ,  $|3\rangle$ . Finally the third regime (III) is formed by the nearest  $\text{TiO}_2$  layer right below SrO, an *orbital-selective metallic* film with comparatively more orbital-balanced character but clearly favoring the  $xy$ -dominated  $|3\rangle$  state in the occupied part. The coherence

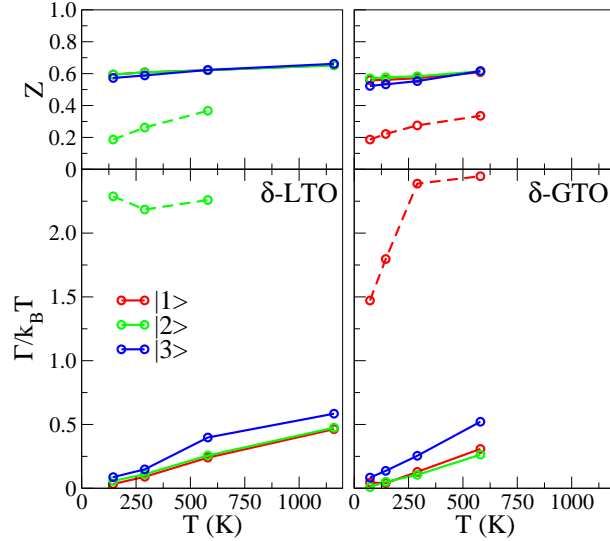


**Figure 8.** Orbital-resolved quasiparticle weight  $Z$  and dimensionless scattering rate  $\Gamma/k_B T$  for the  $\delta$ -doped compounds. Full lines correspond to the states right at the SrO layer and the dashed line to the dominant doped Mott state in the second-distant layer.

of the QPs therein increases significantly at low  $T$ , while the orbital fillings are rather temperature independent. About 0.6 electrons are located at Ti1. The remaining holes are mostly at Ti2, but the hole doping is not fully perfect, i.e. some holes seem to remain within the SrO layer.

Accordingly, the spectral data for  $\delta$ -doped GTO is exhibited in Fig. 7. Since the Curie temperature for ferromagnetic ordering of bulk GTO is well below 100K, we shifted the temperature range and set  $T=73\text{K}$  as the lowest value. In comparison to  $\delta$ -LTO, the QP coherence close to the Fermi level is enlarged, but shows a surprising decline below 100K. In general, the temperature dependence is more delicate in  $\delta$ -doped gadolinium titanate, as can be also seen in the local Ti-resolved  $A(\omega)$ . The three encountered electronic regimes are also present here, now with the corresponding state  $|1\rangle$  as the Mott-dominating one. But for Ti3 and Ti4 there is in addition an  $T$ -dependent transition between regimes I and II. Furthermore the gapped QP of  $|3\rangle$  in the occupied region has a much stronger signature and resides just below the Fermi level. The orbital-occupation character far away from the interface resembles the LTO case, here strongly polarized in the  $|1\rangle$  state with clear  $3d^1$  total filling. Again the strength of orbital polarization is significantly increased compared to the GTO bulk case. Note that here, since the LDA onsite level differences are similar to the bulk, the DMFT self-energy is nearly exclusively responsible for that increase. In general the correlation-induced local level shift renormalizing the original crystal-field splitting is given by  $\Delta_c = \varepsilon_{\text{CSC}} + \text{Re} \Sigma(i0^+) - \Delta_{\text{DC}} - \varepsilon_{\text{cf}}$ . Here  $\varepsilon_{\text{CSC}}$  is the local level energy from the KS-like part in DFT+DMFT,  $\Delta_{\text{DC}}$  is the orbital-independent but site-dependent shift from the fully-localized double counting and  $\varepsilon_{\text{cf}}$  the original crystal-field level energy from LDA. In the close-to-interface regimes II and III there are slight differences, namely marginal depletion of the doped-Mott state at lower  $T$  in II and somewhat

stronger orbital discrimination in III. The total filling at the interface is similar but marginally increased, i.e.  $\text{Ti}^{0.62+}$  compared to  $\text{Ti}^{0.59+}$  in  $\delta$ -doped LTO.

In order to provide insight in the correlation strength within the two metallic layers, Fig. 8 finally shows the QP weight  $Z$  and the dimensionless electron-electron scattering  $\Gamma/k_{\text{B}}T$  for both doped titanates. The data is retrieved from the respective layer-dependent self-energies via  $Z=(1 - \frac{\partial \text{Im} \Sigma(i\omega)}{\partial \omega} |_{\omega \rightarrow 0^+})^{-1} = \frac{m_{\text{LD}} \Delta}{m^*}$  and  $\Gamma = -k_{\text{B}}T Z \text{Im} \Sigma(i0^+)$ . Within the LTO interface layer the QP renormalization is weakly temperature dependent and with  $Z \sim 0.6$  still moderate. Also for the scattering rate the relation  $\Gamma/k_{\text{B}}T < 1$  holds up to high  $T$ , marking the regime III as coherent. Albeit true Fermi-liquid behavior, i.e.  $\Gamma/k_{\text{B}}T$  linear in  $T$ , is only expected for very small temperatures well below the present range, the close-to-linear characteristics is notable. On the other hand the doped-Mott state in the next-distant layer has a stronger  $T$ -dependent QP weight, getting as low as  $Z \sim 0.2$  at  $T=145\text{K}$ . Electron-electron scattering is here severe and strongly incoherent even at low  $T$ . Similar observations hold for  $\delta$ -doped GTO, with overall somewhat increased correlation strength. Interestingly, the incoherent regime II seems on the way of restoring coherency at smaller temperatures, but  $\Gamma/k_{\text{B}}T$  for the similar  $|1\rangle$  character right at the interface deviates from quasi-linear behavior at very low  $T$ .

## 6. Electron states in $\delta$ -doped $\text{GdTiO}_3$ with broken spin symmetry

Finally we discuss possible ordering instabilities in the particle-hole channel. Both bulk materials  $\text{LaTiO}_3$  and  $\text{GdTiO}_3$  exhibit magnetic ordering at low temperatures, but because of the complexity of studying electronic ordering in the doped compounds we here restrict the investigation to only one system, namely the GTO case. In the bulk, the compound becomes ferromagnetic (FM) below 36K and the strongly enhanced spectral weight close to the Fermi level in the  $\delta$ -doped case might be indicative of a Stoner-like magnetic instability. Furthermore, when doped with a SrO monolayer, roughly half of an electron is located at Ti ions right at the doping layer which raises the question about in-plane  $\text{Ti}^{3+}/\text{Ti}^{4+}$  charge ordering [48]. Concerning charge disproportionation or other possible intra-layer instabilities, we performed post-processing (or one-shot) DMFT based on the given projected multi-orbital onsite Hubbard Hamiltonian, now with intra-layer discrimination of the both Ti ions, respectively. However no checkerboard-type or other insulating instability was detected. Nonlocal Coulomb interactions may be relevant to trigger such orderings. A charge self-consistent treatment is not performed since it asks for a symmetry lowering also in the DFT part, which renders the already heavy calculations very expensive. Therefore we still cannot fully exclude the possibility of an insulating solution. In the following we concentrate on broken spin-symmetry and shed light on a possible (in-plane) FM  $\delta$ -doped state from a  $[100]$ - $[010]$  interface architecture. Experimentally, ferromagnetism in  $\text{SrTiO}_3/\text{GdTiO}_3$  quantum wells within a  $[110]$ - $[001]$  interfacing has indeed been reported by Jackson and Stemmer [49].

In principle there are two magnetically active shells in GTO, namely  $\text{Gd}(4f)$  and  $\text{Ti}(3d)$ . Experimental work suggests that in the bulk an antiferromagnetic (AFM) coupling between Gd and Ti sets in at low  $T$ , giving rise to ferrimagnetism [50, 51]. But since the Gd-O-Gd and Gd-O-Ti exchange is believed to be weaker than the (ferromagnetic) Ti-O-Ti one [50], we here approximate the problem by assuming the Gd sites paramagnetic without taking part in the formation of magnetic order. This is reasonable since the temperature  $T=145\text{K}$  is also set way above the bulk  $T_{\text{C}}=36\text{K}$ .

Post-processing (or one-shot) DMFT starting from the charge self-consistent paramagnetic DFT+DMFT solution does not lead to FM order. Using charge-only self-consistency, i.e. neglecting spin polarization in the KS-DFT part, also results in vanishing ordered moments. Only the complete spin-resolved charge self-consistent treatment sustains magnetic order when starting from FM initialization at  $T=145\text{K}$ . Note that the latter protocol may overestimate magnetic-ordering tendencies, because once an exchange-splitting is introduced in KS-DFT via the DMFT Ti1-5 self-energies it may not easily suppressed within the formalism. On the other hand taking into account spin polarization in the KS part may be vital. Moments on the ligands and corresponding exchange is important for the overall lattice magnetic ordering.

A total moment of  $6.8\mu_B$  is obtained for the whole 100-atom supercell with the 20 Ti ions. The material remains in a net metallic regime, as visualized in Fig. 9a when plotting the total spectral function. Both, QP as well as incoherent

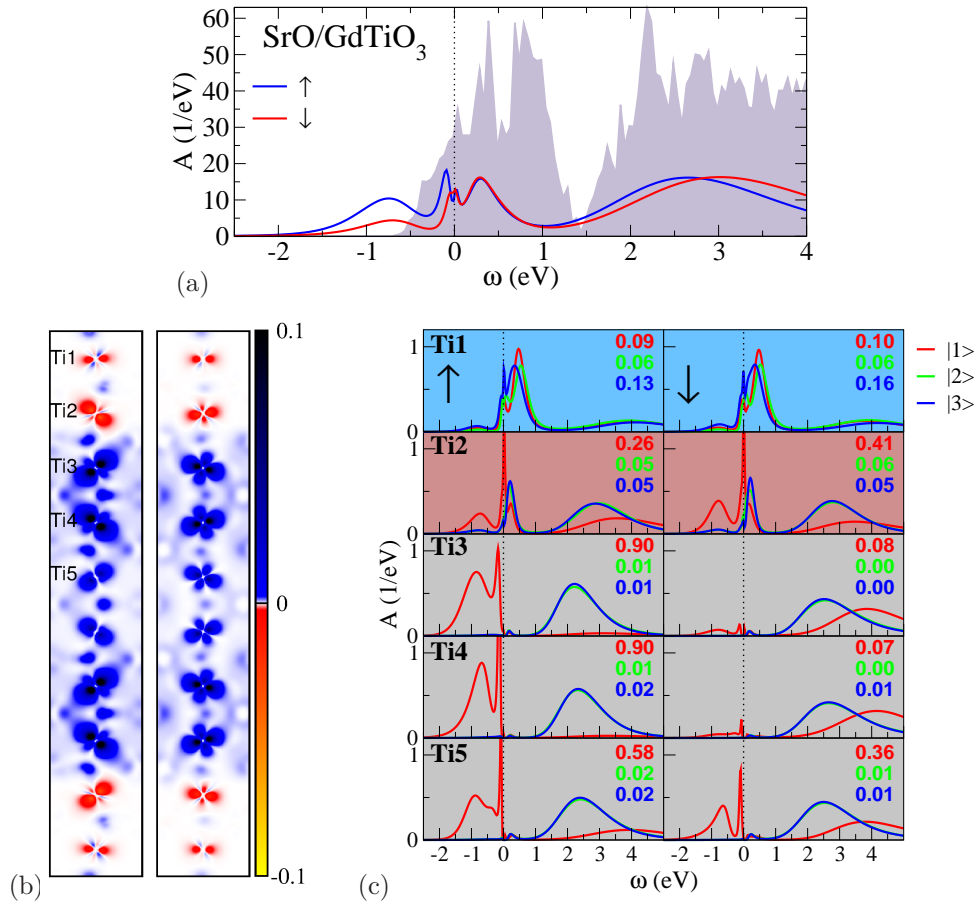


**Figure 9.** Ferrimagnetic  $\delta$ -doped GTO within DFT+DMFT. (a) total spin-resolved spectral function compared to LDA (bluegrey). (b) Spin-resolved charge difference  $\rho_\uparrow - \rho_\downarrow$  within the  $ac$ -plane (left) and the  $bc$ -plane (right). (c) Ti-resolved local spectral function with numbers providing the filling in each orbital-spin channel.

lower Hubbard peak are spin polarized, suggesting a mixed behavior of localized and itinerant ferromagnetism. Second, though initialized as coherent FM, inspecting the real-space ordering interestingly reveals that the system displays at convergence a ferrimagnetic ordering (see Fig. 9b,c). The FM metallic layers with Ti1-2 and the FM Mott-insulating layers with Ti3-5 couple antiferromagnetically, whereby the PM characterization via regimes I-III remains intact in the spin-polarized case. Within the FM orbital-ordered Mott regime the Ti3-4 ions also show nearly complete spin polarization. But the most-distant Ti5 ion surprisingly carries a smaller magnetic moment. Exchange coupling to the metallic FM layers thus seems to increase the ordered moment. These layers in regime II/III are weaker spin polarized, with dominant  $d_{xy}$  weight nearest to the SrO doping layer.

The ferromagnetism in the Mott regime is reminiscent of the corresponding ordering of bulk GTO [12]. In the case of the itinerant  $\text{TiO}_2$  layers, a combined intra- and inter-layer double-exchange-like mechanism [52, 53] may contribute to FM tendencies in the interface region with different structural distortions. For a diverse exchange mechanism therein also speaks the AFM coupling of Ti to the apical oxygens (cf. Fig. 9b), whereas in the Mott layers these ligands appear FM coupled to the titanium ions. The reason for the AFM coupling of both parts appears more subtle. On the basis of the Goodenough-Kanamori rules [54, 55], it could be related to the 'more 180°-like' orientation of the nearby Ti2-3  $|1\rangle$  orbitals, evident from the weaker rotation in the  $bc$ -plane on Ti2 compared to Ti4 in Fig. 9b. The total-energy competition between the paramagnetic and ferrimagnetic state is rather tight, favoring the magnetic order by about 10 meV/atom.

## 7. Summary and Discussion

Starting from the Mott-insulating bulk compounds  $\text{LaTiO}_3$  and  $\text{GdTiO}_3$  we investigated the rich and complex electronic structure originating from  $\delta$ -doping with an SrO monolayer in a superlattice architecture along the [001] direction. The realistic multi-orbital setup with 10  $\text{TiO}_2$  layers inbetween the doping layers allows to differentiate various correlation regimes with distance to SrO by the elaborate DFT+DMFT method. An orbital-selective itinerant state at the interface changes into an itinerant orbital-polarized doped-Mott state, which transforms to an orbital-ordered Mott-insulating region at larger distance. Notably that Mott regime displays even stronger orbital polarization than the bulk-insulating case. The transport within the itinerant layers is of mixed Fermi-liquid-like- and incoherent character. Generally the  $\delta$ -doped GTO case promotes somewhat stronger correlation effects than  $\delta$ -doped LTO above the respective ordering temperatures.

Our study reveals the intricate interplay between structural distortions and the electrons' charge, orbital, spin degrees of freedom in the heterostructure. The layer- and temperature-dependent transitions between the encountered electronic phases pose novel challenging problems in strongly correlated electron systems. For instance, further theoretical investigations are necessary to shed light on the dependence on the number of SrO layers. Concerning comparison with experiment, our concrete work serves as a theoretical prediction, since to our knowledge the here here studied canonical [100], [010] interface geometry for  $\delta$ -doped titanates has so far not been experimentally investigated. There are recent experimental works on [110], [001] interfaces [42, 8, 43] that find an overall insulating state for  $\delta$ -GTO. This different finding may indeed be traced back to the differences in the interface geometries.



Whereas the ([100],[010]) interface is nearly perfectly flat in our calculation, the ([110],[001]) one shows some buckling [42], which we can confirm [56]. Note that due to the different orientations, the square-like interface Ti sublattice has much stronger rectangular distortion in the ([110],[001]) geometry. This could more easily trigger the  $\text{Ti}^{3+}/\text{Ti}^{4+}$ -like charge ordering as one option to form the insulating interface state. Furthermore the distinct orbital-ordering in Mott-insulating titanates is not easily commensurate across the ([110],[001]) geometry, which might lead to a symmetry-breaking of the original GTO orbital ordering based on the  $|1\rangle$  state aligned predominantly along the  $a$ -axis.

Allowing for spin ordering results in a further enrichment of the already sophisticated electronic structure. A ferrimagnetic ordering, again with itinerant and Mott-insulating regimes, settles in  $\delta$ -doped GTO. It results from the subtle exchange-interaction variations due to the differences in structural distortions, orbital occupations as well as degree of itinerancy.

The present work renders it obvious that the electronic structure characteristics in oxide heterostructures are in principle likely to cover the full plethora of many-body condensed matter physics within a single (designed) compound. From another perspective, this generates vast room for engineering and creating novel states of matter.

## Acknowledgments

We are grateful to S. Stemmer and L. Balents for helpful discussions. Calculations were performed at the Juropa Cluster of the Jülich Supercomputing Centre (JSC) under project number hhh08. This research was supported by the DFG-FOR1346 project.

## References

- [1] Zubko P, Gariglio S, Gabay M, Ghosez P and Triscone J M 2011 *Annu. Rev. Condens. Matter Phys.* **2** 141
- [2] Hwang H Y, Iwasa Y, Kawasaki M, Keimer B, Nagaosa N and Tokura Y 2012 *Nature Materials* **11** 103
- [3] Chakhalian J, Freeland J W, Millis A J, Panagopoulos C and Rondinelli J M 2014 *Rev. Mod. Phys.* **86** 1189
- [4] Kim J S, Seo S S A, Chisholm M F, Kremer R K, Habermeier H U, Keimer B and Lee H N 2010 *Phys. Rev. B* **82** 201407(R)
- [5] Jang H W, Felker D A, Bark C W, Wang Y, Niranjana M K, Nelson C T, Zhang Y, Su D, Folkman C M, Baek S H, Lee S, Janicka K, Zhu Y, Pan X Q, Fong D D, Tsymbal E Y, Ryzhowski M S and Eom C B 2011 *Science* **331** 886
- [6] Choi W S, Lee S, Cooper V R and Lee H N 2012 *Nano Lett.* **12** 4590
- [7] Rastogi A, Pulikkotil J J and Budhani R C 2014 *Phys. Rev. B* **89** 125127
- [8] Ouellette D G, Moetakef P, Cain T A, Zhang J Y, Stemmer S, Emin D and Allen S J 2013 *Scientific Reports* **3** 3284
- [9] Chen R, Lee S B and Balents L 2013 *Phys. Rev. B* **87** 161119(R)
- [10] Lechermann F, Boehnke L and Grieger D 2013 *Phys. Rev. B* **87** 241101(R)
- [11] Jackson C A, Zhang J Y, Freeze C R and Stemmer S 2014 *Nat. Commun.* **5** 4258
- [12] Komarek A C, Roth H, Cwik M, Stein W D, Baier J, Kriener M, Bourée F, Lorenz T and Braden M 2007 *Phys. Rev. B* **75** 224402
- [13] Goral J P and Greedan J E 1983 *J. Magn. Magn. Mater.* **37** 315
- [14] Amow G and Greedan J E 1996 *J. Solid State Chem.* **121** 443
- [15] Onoda M and Yasumoto M 1997 *J. Phys.: Condens. Matter* **9** 3861
- [16] Hays C C, Zhou J S, Markert J T and Goodenough J B 1999 *Phys. Rev. B* **60** 10367

- [17] Keimer B, Casa D, Ivanov A, Lynn J W, v Zimmermann M, Hill J P, Gibbs D, Taguchi Y and Tokura Y 2000 *Phys. Rev. Lett.* **85** 3946
- [18] Khaliullin G and Maekawa S 2000 *Phys. Rev. Lett.* **85** 3950
- [19] Solovyev I V 2004 *Phys. Rev. B* **69** 134403
- [20] Moshizuki M and Imada M 2001 *J. Phys. Soc. Jpn.* **70** 2872
- [21] Pavarini E, Biermann S, Poteryaev A, Lichtenstein A I, Georges A and Andersen O K 2004 *Phys. Rev. Lett.* **92** 176403
- [22] Craco L, Laad M S, Leoni S and Müller-Hartmann E 2004 *Phys. Rev. B* **70** 195116
- [23] Pavarini E, Yamasaki A, Nuss J and Andersen O K 2005 *New J. Phys.* **7** 188
- [24] Iori F, Gatti M and Rubio A 2012 *Phys. Rev. B* **85** 115129
- [25] Assmann E, Blaha P, Laskowski R, Held K, Okamoto S and Sangiovanni G 2013 *Phys. Rev. Lett.* **110** 078701
- [26] Louie S G, Ho K M and Cohen M L 1979 *Phys. Rev. B* **19** 1774
- [27] Meyer B, Elsässer C, Lechermann F and Fähnle M unpublished *FORTTRAN 90 Program for Mixed-Basis-Pseudopotential Calculations for Crystals* Max-Planck-Institut für Metallforschung, Stuttgart
- [28] Savrasov S Y, Kotliar G and Abrahams E 2001 *Nature* **410** 793
- [29] Pourovskii L V, Amadon B, Biermann S and Georges A 2007 *Phys. Rev. B* **76** 235101
- [30] Grieger D, Piefke C, Peil O E and Lechermann F 2012 *Phys. Rev. B* **86** 155121
- [31] Anisimov V I, Kondakov D E, Kozhevnikov A V, Nekrasov I A, Pchelkina Z V, Allen J W, Mo S K, Kim H D, Metcalf P, Suga S, Sekiyama A, Keller G, Leonov I, Ren X and Vollhardt D 2005 *Phys. Rev. B* **71** 125119
- [32] Amadon B, Lechermann F, Georges A, Jollet F, Wehling T O and Lichtenstein A I 2008 *Phys. Rev. B* **77** 205112
- [33] Haule K, Yee C H and Kim K 2010 *Phys. Rev. B* **81** 195107
- [34] Rubtsov A N, Savkin V V and Lichtenstein A I 2005 *Phys. Rev. B* **72** 035122
- [35] Werner P, Comanac A, de' Medici L, Troyer M and Millis A J 2006 *Phys. Rev. Lett.* **97** 076405
- [36] Ferrero M and Parcollet O TRIQS: a Toolbox for Research in Interacting Quantum Systems URL <http://ipht.cea.fr/triqs>
- [37] Boehnke L, Hafermann H, Ferrero M, Lechermann F and Parcollet O 2011 *Phys. Rev. B* **84** 075145
- [38] Solovyev I V, Dederichs P H and Anisimov V I 1994 *Phys. Rev. B* **50** 16861
- [39] Haule K, Biroli T and Kotliar G 2014 *Phys. Rev. B* **90** 075136
- [40] Dang H T, Millis A J and Marianetti C A 2014 *Phys. Rev. B* **89** 161113(R)
- [41] Park H, Millis A J and Marianetti C A 2012 *Phys. Rev. Lett.* **109** 156402
- [42] Zhang J Y, Hwang J, Raghavan S and Stemmer S 2013 *Phys. Rev. Lett.* **110** 256401
- [43] Zhang J Y, Jackson C A, Chen R, Raghavan S, Moetakef P, Balents L and Stemmer S 2014 *Phys. Rev. B* **89** 075140
- [44] Lechermann F, Georges A, Poteryaev A, Biermann S, Posternak M, Yamasaki A and Andersen O K 2006 *Phys. Rev. B* **74** 125120
- [45] Crandles D A, Timusk T, Garrett J D and Greedan J E 1992 *Physica C* **201** 407
- [46] Arima T, Tokura Y and Torrance J B 1993 *Phys. Rev. B* **48** 17006
- [47] Okimoto Y, Katsufuji T, Okada Y, Arima T and Tokura Y 1995 *Phys. Rev. B* **51** 9581
- [48] Pentcheva R and Pickett W E 2007 *Phys. Rev. Lett.* **99** 016802
- [49] Jackson C A and Stemmer S 2013 *Phys. Rev. B* **88** 180403(R)
- [50] Turner C W and Greedan J E 1980 *J. of Solid State Chem.*
- [51] Zhou H D and Goodenough J B 2005 *J. Phys.: Condens. Matter* **17** 7395
- [52] Zener C 1951 *Phys. Rev.* **82** 403
- [53] Anderson P W and Hasegawa H 1955 *Phys. Rev.* **100** 675
- [54] Goodenough J B 1963 *Magnetism and the Chemical Bond* (Interscience, New York)
- [55] Kanamori J 1959 *J. Phys. Chem. Solids* **10** 87
- [56] Lechermann F to be published